JOURNAL OF Materials CHEMISTRY

Control of structure, pore size and morphology of three-dimensionally ordered mesoporous silicas prepared using the dicationic surfactant $[CH_3(CH_2)_{15}N(CH_3)_2(CH_2)_3N(CH_3)_3]Br_2$†

Alfonso E. Garcia-Bennett,[a] Sylvia Williamson,[a] Paul A. Wright*[a] and Ian J. Shannon[b]

[a]*School of Chemistry, University of St Andrews, Purdie Building, North Haugh, St Andrews, Fife, UK KY16 9ST. E-mail: paw2@st-andrews.ac.uk*
[b]*Department of Chemical Sciences, University of Birmingham, Edgbaston, Birmingham, UK B15 2TT*

Received 6th June 2002, Accepted 10th September 2002
First published as an Advance Article on the web 29th October 2002

The synthesis of mesoporous silicas in the presence of the dicationic gemini surfactant $[CH_3(CH_2)_{15}N(CH_3)_2(CH_2)_3N(CH_3)_3]Br_2$ (C16-3-1) has been investigated at low temperatures (−4 °C) under basic and acidic conditions. Under basic conditions, the SBA-2 phase (based on a close-packed arrangement of micelles and exhibiting frequent stacking faults) is observed, with hollow sphere morphology. Under strongly acidic conditions, the phase SBA-1 ($Pm\bar{3}n$) and the SBA-2 family of phases (based on the close packing of micelles) are observed, depending on the surfactant and silicate content of the original gel. Conditions under which the pure hexagonally close-packed end member of the family ($P6_3/mmc$) is formed have been identified. SBA-1 and the pure hexagonally close-packed end member are prepared with well-defined morphologies. The adsorption of nitrogen and the hydrocarbons cyclopentane and mesitylene reveal that SBA-2 prepared in basic media has a cage structure where the cages are linked through small (<4 Å) micropores, whereas the silicas prepared in acidic media have larger pores after calcination. SBA-1 and a poorly ordered SBA-2, prepared using C16-3-1 under acidic conditions, are able to adsorb mesitylene (diameter *ca.* 8 Å), whereas the hexagonal end member of the SBA-2 series prepared under acidic conditions is able to adsorb cyclopentane (diameter *ca.* 5 Å) but not mesitylene.

Introduction

More than a decade after the discovery of the two-dimensionally ordered hexagonal mesoporous silica MCM-41,[1,2] a great deal of research has examined the synthesis, characterisation and potential catalytic applications of this solid[3–5] and the similar material SBA-15 (Santa Barbara-15), which possesses the same symmetry (*p6mm*), but is prepared using non-ionic, rather than cationic, surfactants.[6] Over the same period, four well-defined composite silica–surfactant mesophases that possess structures that exhibit three-dimensional order have been prepared: MCM-48 ($Ia\bar{3}d$),[2,7–9] SBA-1 and the similar SBA-6 ($Pm\bar{3}n$),[10–13] SBA-2 and the similar SBA-12 ($P6_3/mmc$ and intergrowth structures),[10,11,14–16] and SBA-16 ($Im\bar{3}m$).[6] Each of these structure types display characteristic low angle X-ray diffraction patterns and have been characterised by electron microscopy, structural modelling combined with simulation of the X-ray diffraction pattern, and electron crystallography.[17,18]

The mesoporous materials SBA-1 and SBA-2 were first synthesised in 1995 and 1996, respectively, by Huo and co-workers.[10,11] SBA-1 and SBA-2 (and similar structures) may be considered to be made up of silicate cages that are formed by condensation around spherical micelles. The average structures of these two types of structure, as determined by electron crystallography, have been reported by Terasaki and co-workers.[17,18]

SBA-1 is typically prepared under acidic conditions using the surfactant cetyltriethylammonium bromide (CTEABr). The structure of SBA-1 involves two kinds of cages, larger A cages (diameter *ca.* 40 Å from electron crystallography studies) and smaller B cages (diameter *ca.* 33 Å) in the ratio 3 : 1.[19] Pure silica SBA-1 is typically prepared under acidic conditions using the cetyltriethylammonium cation as a surfactant. Recent reports show that silica–surfactant mesophases occur under strongly acidic conditions *via* the formation of $S^+X^-I^+$ micelles, where S^+ denotes the surfactant cation, X^- the anion and I^+ the silica species. The concentration of I^+ involved in the formation of the surfactant micelles increases with increasing acidity, as a result of proton adsorption. The high concentration of HCl in the starting mixture is thought to cause an increase in the ratio of the volume of the surfactant head group to that of the hydrocarbon tail that, in turn, favours the formation of spherical micelles and the cubic SBA-1 mesophase.[19]

The SBA-2 and SBA-12 families of structures, which show strong structural similarities,[12] are thought to be based on close-packed arrays of spherical micelles which display both hexagonal (hcp) and cubic close packing (ccp) sequences. Evidence for this includes the fact that the *c*/*a* ratio of the unit cell of predominantly hexagonal SBA-2 approaches 1.63, the ideal ratio for hcp stacking of spheres, and electron microscopy studies.[14] SBA-2 is typically prepared from syntheses under basic conditions[10,20] using the dicationic surfactant $[CH_3(CH_2)_{15}N(CH_3)_2(CH_2)_3N(CH_3)_3]Br_2$ (C16-3-1), whereas SBA-12 is prepared under acidic conditions using the non-ionic Brij-76 surfactant. Related non-ionic $C_{12}EO_8$ surfactants have been observed to form the 3-D hexagonal liquid crystalline mesophase in aqueous solution.[21,22] The curvature associated with the internal surfaces of these solids is high, and so these structures are thought to be favoured by surfactants with

†Electronic supplementary information (ESI) available: mesitylene, cyclopentane and nitrogen adsorption–desorption isotherms for calcined mesoporous samples. See http://www.rsc.org/suppdata/jm/b2/b205470c/

large head groups, such as the dicationic surfactants of the general form C*m*-*n*-1, as described above. Nitrogen adsorption measurements on these materials have shown that the 'mesocage' diameter is well defined and varies between 25 and 40 Å,[11,14] as estimated by BJH (Barret–Joyner–Halenda) analysis,[23] according to the synthesis conditions.[10] The total pore volume of SBA-2, as measured by nitrogen adsorption, is lower than expected for full connection of close-packed spherical cages. The size and number of connections between these cages is not yet well understood.

Examples of thin silicate films with the 3-D hexagonal ($P6_3/mmc$) structure have been prepared under acidic synthesis conditions, with the *c*-axis perpendicular to the plane of the film.[24–26] In addition, the mesostructured SBA-12, which is prepared under acidic conditions using non-ionic surfactants, is found to have a similar structure to SBA-2 and detailed electron crystallographic studies[18] have revealed a pore structure where each pore is surrounded by twelve others with a pore diameter estimated at 24 Å. Again, however, nitrogen uptakes are lower than expected.

In this study, we have examined the use of C16-3-1 as a surfactant template, concentrating on syntheses at low temperature and under acidic conditions that have been shown by others to be effective in preparing samples of SBA-1 with well-defined 'crystal' morphologies using CTEABr. Under these conditions, the silicate condensation is thought to proceed slowly with respect to formation of the mesophase, allowing the surfactant–silicate composite time to achieve favoured 'crystalline' morphologies. We have also examined the use of aqueous solutions with surfactant concentrations of up to 50 wt% in preparation of the gels in an attempt to investigate phase variation in the acidified [SiO_2–H_2O–C16-3-1] compositional space. These studies show clear trends in the resultant phases and their morphologies, and reveal that 3-D hexagonal and cubic phases are produced, including materials with $P6_3/mmc$ and $Pm\bar{3}n$ symmetry.

The pore sizes for these solids are usually estimated from nitrogen adsorption data. Use of the widely available BJH model typically gives pore diameter values of 20–40 Å for these 'mesocage' materials. More recently, Ravikovitch and co-workers[27,28] have used non-local density functional theory (NLDFT) to estimate the pore diameters more accurately. These calculations suggest that the BJH methods underestimate the pore diameters by 30–40%.[27] All analyses of this kind give values for the pore diameter but do not give window sizes. We have therefore measured the adsorption of hydrocarbon vapours, *n*-hexane, cyclopentane and 1,3,5-trimethylbenzene (mesitylene), within the pores of the mesoporous silicas prepared using C16-3-1 in order to determine directly limits to the sizes of the pores joining the 'mesocages', rather than their pore diameters. This approach gives results that are important for the potential applications of these solids as catalysts and adsorbents.

Experimental

Syntheses

SBA-2 was prepared under basic conditions using the method of Huo *et al*,[10] as previously described,[14,15] at room temperature (referred to below as SBA-2RT). SBA-2 was also synthesised under basic conditions at low temperature (−4 °C; SBA-2LT). In a typical preparation of SBA-2LT, a 1 wt% solution of the gemini surfactant $CH_3(CH_2)_{15}N(CH_3)_2(CH_2)_3$-$N(CH_3)_3Br_2$ (C16-3-1)[29] was added to an aqueous solution of tetramethylammonium hydroxide (TMAOH, 25 wt%, Aldrich), followed by dropwise addition of tetraethyl orthosilicate, (TEOS, Aldrich), to give a final TEOS : C16-3-1 : H_2O : TMAOH molar ratio in the gel of of 1 : 0.3 : 85 : 0.5. The solution was stirred for a period of 5 min at 300 rpm to promote the hydrolysis of the silicate. The reaction gel was then allowed to stand at −4 °C for 3 days with no stirring. After the reaction, the SBA-2 precipitate was filtered off, washed with distilled water and dried overnight in air at room temperature.

Synthesis of mesophase materials was carried out under acidic conditions starting with aqueous solutions of C16-3-1 at various concentrations and using different silicate concentrations in the presence of 20 wt% surfactant solution. Initial optical microscopic investigations of the behaviour of aqueous solutions of C16-3-1 at room temperature showed that a succession of liquid crystalline phases are obtained (Table 1), so it was decided to investigate this range of concentrations in the synthesis of mesoporous silicas. The appropriate amount of C16-3-1 surfactant was dissolved in distilled water, followed by addition of aqueous HCl (37 wt%, Aldrich), and the reaction stirred for 30 min to obtain a homogeneous solution. TEOS was introduced dropwise under continuous stirring and the mixture was stirred for a further 5 min before allowing the reaction to continue, without stirring, at −4 °C for 3 days. The resulting white precipitate was filtered off without washing and dried at 100 °C overnight. The final molar compositions of these reaction mixtures are summarised in Table 2.

A further series of syntheses were performed using a fixed concentration of surfactant, but varying the molar quantity of TEOS added to the gel (Table 3).

For all samples, removal of the surfactant was effected by calcination at 550 °C (1 h in N_2, followed by 6 h in O_2), to give the porous silicate.

Characterisation

Powder X-ray diffraction patterns were collected at ambient temperature using Cu-K_α radiation (λ = 1.5418 Å) on a Philips PW 1830 diffractometer equipped with a secondary monochromator. Scanning electron microscopy (SEM) images were obtained using a JEOL JSM-5600 scanning electron microscope operating at voltages of up to 30 kV and with an optimal resolution of 3 nm. HRTEM images were recorded using a JEOL JEM-200CX electron microscope operating at 200 kV.

Table 1 Observed liquid crystalline phase transitions of surfactant C16-3-1 in water at different surfactant concentrations and at room temperature. The different solutions were allowed to equilibrate at room temperature for 1 week before transferring them to an optical polarising microscope slide. Phases are proposed on the basis of the texture, fluidity and presence (or otherwise) of birefringence in the observed phase

Surfactant concentration (wt%)	Observations at room temperature	Interpretation
10	No liquid crystalline phase observed.	—
20	Formation of a viscous non-birefringent phase and a fluid birefringent phase.	Cubic (non-birefringent) and hexagonal (birefringent).
40	Formation of a birefringent liquid crystalline phase that flows with ease. A minor birefringent phase with a more viscous texture is also observed.	Hexagonal phase(s).
60	Viscous gel-like birefringent phase forming distorted bubbles, with the appearance of small regions of a non-birefringent phase.	Hexagonal phase with small regions of a cubic (non-birefringent) phase.
80	Single viscous birefringent liquid crystalline phase.	Hexagonal phase.

Table 2 Summary of conditions and molar compositions for reactions using various concentrations of C16-3-1 under acidic conditions at −4 °C

Surfactant concentration (wt%)	Final TEOS : C16-3-1 : H_2O : HCl molar ratio	Morphology	Phase formed	XRD unit cell parameters (calcined)/Å
1	1 : 0.018 : 55 : 6	Amorphous	Undetermined	—
10	1 : 0.18 : 55 : 6	Spherical	SBA-2/STAC-1	$a = 41$, $c = 65$
20	1 : 0.37 : 55 : 6	Dodecahedra/blocks	Mixed phase	—
30	1 : 0.56 : 55 : 6	Dodecahedra/blocks	Mixed phase	—
40	1 : 0.75 : 55 : 6	Hexagonal prisms	STA-10	$a = 43$, $c = 68$
50	1 : 0.94 : 55 : 6	Amorphous	Wormhole	—

Table 3 Summary of conditions and molar compositions for reactions using 20 wt% C16-3-1 and various TEOS concentrations under acidic conditions at −4 °C[a]

TEOS/C16-3-1 (wt%)	Final TEOS : C16-3-1 : H_2O : HCl molar ratio	Phase formed	XRD unit cell parameters (calcined)/Å
100	1 : 0.37 : 55 : 6	Mixed phase	—
80	0.8 : 0.37 : 55 : 6	Mixed phase	—
60	0.6 : 0.37 : 55 : 6	SBA-1	$a = 83$
40	0.4 : 0.37 : 55 : 6	SBA-1	$a = 79$

[a]For comparison; SBA-1(CTEABr) $a = 74$ Å.

Samples were prepared by deposition onto holey carbon films, supported on a Cu grid, before transferring them into the specimen chamber. The objective lens parameters, $C_S = 0.41$ nm and $C_C = 0.95$ nm, gave an interpretable point resolution of *ca.* 1.85 Å. Images were recorded along high symmetry zone axes at magnifications of 24000× to 49000×. It was found that the as-prepared samples decomposed in the electron beam, thus, all HRTEM investigations are based on calcined samples. The fine powders were ground prior to deposition onto the TEM specimen grid.

Direct polarisation (DP) MAS ^{29}Si NMR was carried out on a Varian UNITYI/nova spectrometer with a 7.05 T Oxford Instruments magnet, using a pulse angle of 90.0°, an acquisition time of 10.0 ms and a relaxation delay of 120.0 s.

Nitrogen adsorption–desorption isotherms were measured at 77 K using an IGA-2 series gravimetric analyser. Samples were degassed at 250 °C overnight at $\sim 4 \times 10^{-3}$ Torr prior to measuring the isotherm. Adsorption values were measured gravimetrically and, for each step, the increase in weight was followed as a function of time. Each step was permitted to approach equilibrium over a period of 90 min, and a full experiment (adsorption and desorption) typically comprised some 50 steps over 24 h. Measurements of specific area are based on the Brunauer–Emmett–Teller (BET) method, which is generally applicable to Type II isotherms and may be applicable to Type IV isotherms at pressures below those at which capillary condensation occurs. In the case of 'mesocage' solids, these values should only be used for comparative purposes. NLDFT software (the most recent method for the determination of pore sizes of spherical connected pores) was not available to us. In order to obtain values for comparative purposes, BJH software provided with the IGA-2 gravimetric analyser was used on desorption data where the calculated pore diameters are greater than 20 Å. For diameters less than 20 Å, the Kelvin equation underlying the BJH calculation is no longer applicable and the Dubinin–Astakhov (DA) model for the analysis of the filling of the micropores is used. Although not directly comparable with the BJH values, the DA results are included for completeness. Cyclopentane (99.9%, Fluka) and mesitylene (99.9%, Fluka) adsorption–desorption isotherms were measured at 5 and 20 °C, respectively, using the IGA-2 gravimetric analyser.

Results and discussion

Results from the following series of syntheses are reported: firstly, the effect of lowering the temperature on the products of synthesis in basic media, secondly, the effect of increasing the concentrations of surfactant on the mesoporous silica product in acidic media and, thirdly, the effect of changing silicate concentration at a constant surfactant concentration, also under acidic conditions.

Fig. 1 shows powder X-ray diffraction profiles of samples of SBA-2 synthesised at room temperature and at low temperature (−4 °C) under basic conditions; both are characteristic of SBA-2 samples and may be indexed on the basis of a hexagonal unit cell. Typically, for calcined samples, $a = 57$, $c = 92$ Å for SBA-2RT and $a = 46$, $c = 75$ Å for SBA-2LT. A similar variation in unit cell dimensions was observed previously among SBA-2 materials prepared using basic solutions with the pH varied between 10 and 12.[20] The SEM image of SBA-2LT [Fig. 2(a)] reveals hollow spheres similar to those reported previously.[15] A larger number of spherical particles are observed in the samples synthesised at low temperature, with an average particle size of *ca.* 80 μm. This may be attributed to the slower growth of the particles as a result of the low temperatures employed in the synthesis, *i.e.* slower self-assembly of the surfactant phase and, therefore, slower formation of the particle morphology.

The N_2 adsorption isotherms for SBA-2RT (Fig. 3) and SBA-2LT are similar in shape to those reported elsewhere,[20] although the sample prepared at low temperature has a reduced

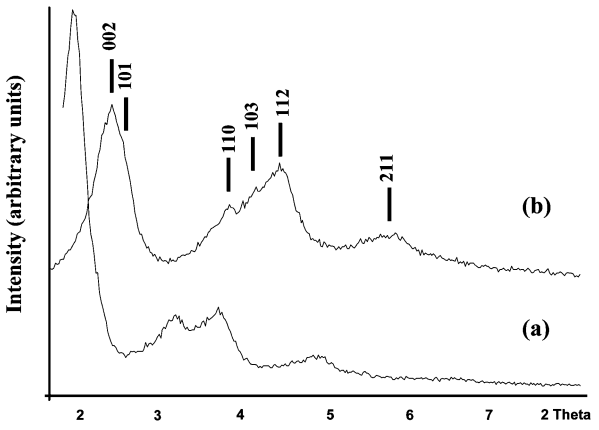

Fig. 1 XRD patterns of SBA-2 prepared under basic conditions at (a) room temperature (SBA-2RT) and (b) −4 °C (SBA-2LT). Both patterns can be indexed on the basis of a hexagonal unit cell ($P6_3/mmc$). For SBA-2RT, $a = 57$, $c = 97$ Å; for SBA-2LT, $a = 46$, $c = 75$ Å.

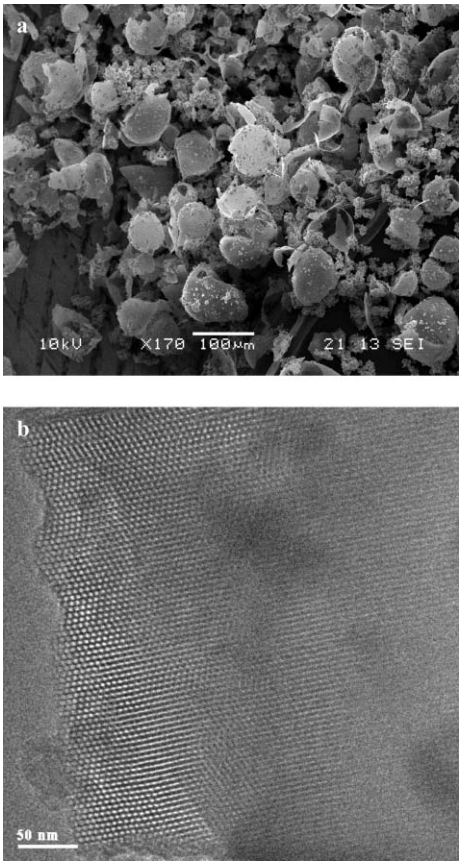

Fig. 2 (a) SEM image showing broken, hollow spherical particles. (b) Under-focused HRTEM image along the [100] direction showing typical stacking faults encountered in calcined SBA-2LT.

total pore volume and adsorption on this sample takes longer to reach equilibrium. BET surface areas, BJH pore sizes and pore volumes are given in Table 4. We can conclude that a reduction in pore volume, pore size and surface area is observed when SBA-2 is synthesised at lower temperatures (consistent with the decrease in the unit cell parameters of the calcined materials). Adsorption of *n*-hexane, cyclopentane and mesitylene on these two solids is low (<10 wt%) compared to the nitrogen uptake. This confirms the previously suggested model for SBA-2 in which the window size between the cages is much smaller than the diameter of the cage.[14] We can conclude from the molecular dimensions of *n*-hexane that most of these connections have a diameter of less than 4 Å. This is the first direct evidence of the window size in SBA-2 prepared under basic conditions. It is worth noting that recent reports in the literature[30] suggest that all mesoporous materials must contain a degree of microporosity in order to account for the large surface areas measured.

The HRTEM image of SBA-2LT [Fig. 2(b)] shows structural characteristics typical of SBA-2 described by Zhou *et al.*[14] (the presence of domains of the cubic polymorph STAC-1 and stacking faults). Contrast profile analysis of lines through the centre pore channels were conducted on good quality HRTEM images looking down high symmetry zone axes using the software package Digital Micrograph[31] (Table 4). The pore sizes estimated by measuring distances between points at half the peak height in the contrast curves are in agreement with our N_2 adsorption–desorption isotherm data, and a decrease in pore size is also found when the synthesis of SBA-2 is carried out at low temperatures.

Powder XRD patterns for samples synthesised in strongly acidic media and at low temperatures are shown in Fig. 4. The C16-3-1 surfactant concentration was varied from 1 to 50 wt%. All samples show peaks between 2–4° 2θ, typical of

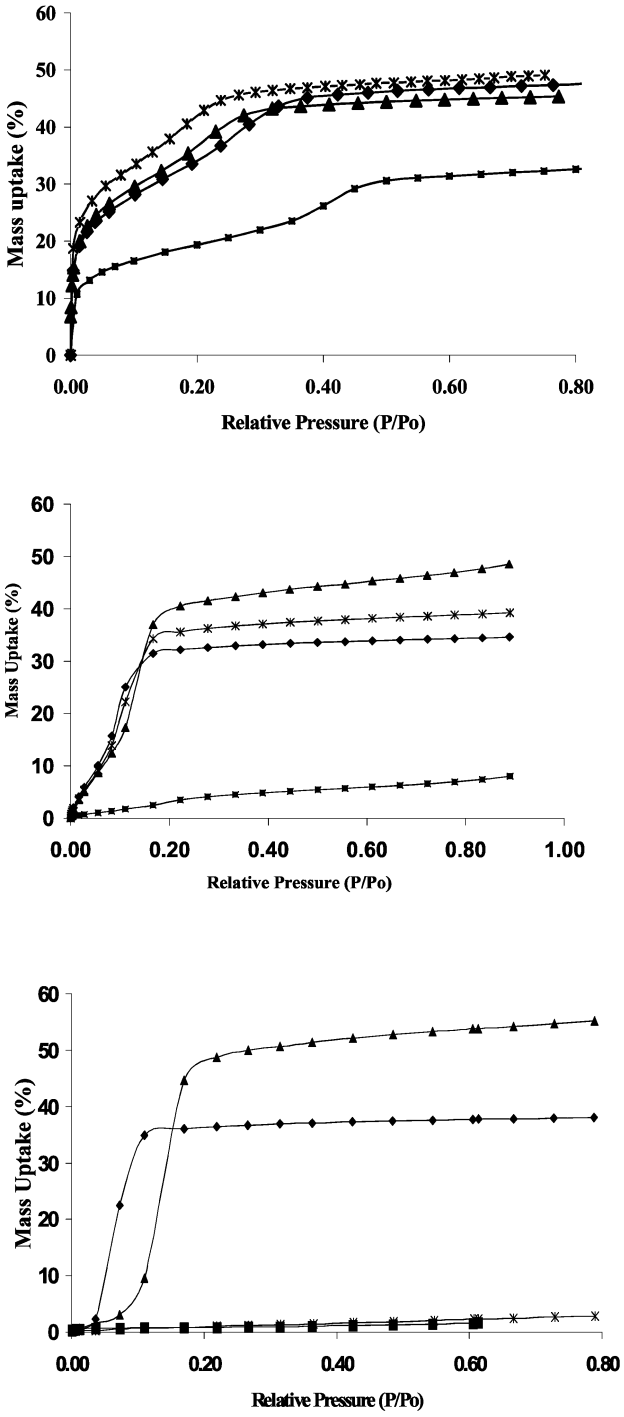

Fig. 3 N_2 adsorption isotherms at 77 K (top), cyclopentane adsorption isotherms at 278 K (middle) and mesitylene adsorption isotherms at 293 K (bottom) of mesoporous materials prepared under acidic and basic conditions. Key: (◆) SBA-2(acid); (▲) SBA-1(C16-3-1); (*) STA-10; (■) SBA-2RT.

'mesoporous' materials. For materials synthesised with 1 and 50 wt% surfactant concentrations however, peaks in this region are considerably lower than for the other samples. This is associated with a decrease in the order of the material, which is also highlighted by the lack of definition of peaks at higher angles (4–7° 2θ). TEM analysis of the sample prepared at 1 wt% surfactant concentration revealed long range ordering of the pores, whereas the sample prepared with 50 wt% surfactant concentration possesses a highly disordered pore structure (micrographs not shown).

Samples synthesised using surfactant concentrations between

Table 4 Porosity data from nitrogen adsorption measurements and transmission electron microscopy for mesoporous materials prepared under acidic and basic conditions

Sample	S_{BET}[a]/m^2 g^{-1}	Pore volume/cm^3 g^{-1}	Average pore size distribution[b]/Å	Pore size (TEM)/Å	Pore wall (TEM)/Å
SBA-2RT	719	0.40	30	32	13.4
SBA-2LT	555	0.14	23	24	15
SBA-2(acid)	1030	0.56	(18)	25	14
Mixed phase (20 wt%)	870	0.40	(16)	29	12
STA-10	1109	0.60	(18)	22	10
SBA-1(C16-3-1)	1086	0.56	22	31	6
SBA-1(CTEABr)	1100	0.65	15	22	18

[a]BET values included for comparison with other literature reports. [b]Average pore size (diameter) calculated from desorption branches of N_2 isotherms using the BJH (for values >20 Å) or Dubinin–Astakhov[33] (values in parentheses) models.

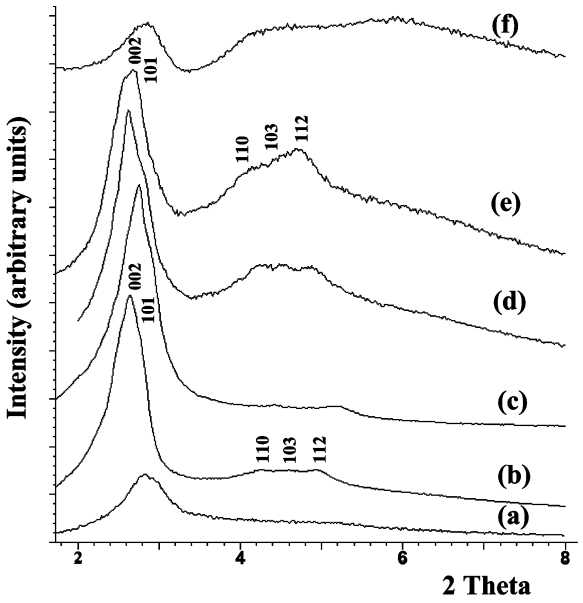

Fig. 4 Powder XRD patterns of calcined mesoporous materials synthesised with (a) 1, (b) 10, (c) 20, (d) 30, (e) 40 and (f) 50 wt% C16-3-1 surfactant concentration, at −4 °C under acidic conditions.

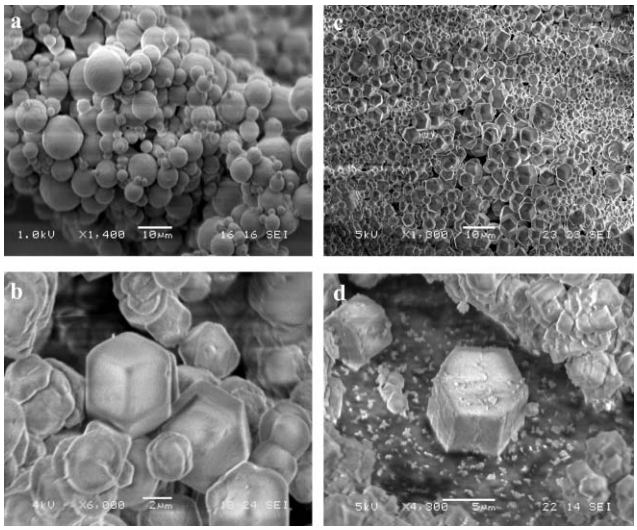

Fig. 5 Typical SEM images of particle morphologies of calcined mesoporous samples synthesised with C16-3-1 surfactant concentrations of (a) 10, (b) 20, (c) 30 and (d) 40 wt%, at −4 °C under acidic conditions.

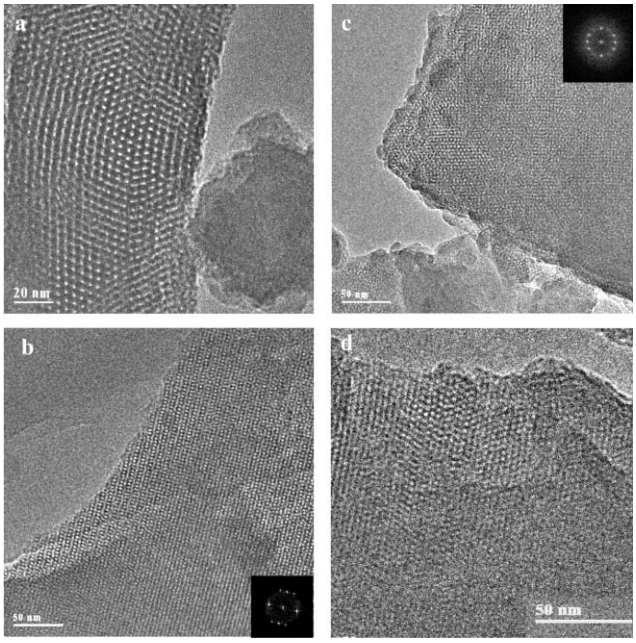

Fig. 6 Typical under-focused HRTEM images of calcined mesoporous materials synthesised with C16-3-1 surfactant concentrations of (a) 10, (b) 20 (view along the [210] direction; the inset shows the FT diffraction pattern of a selected area of the image), (c) 30 (view along the [210] direction; the inset shows the inverse FT diffraction pattern of a selected area of the image) and (d) 40 wt%, at −4 °C under acidic conditions.

10 and 40 wt% display X-ray reflections that are better defined, particularly over the range 3.5–7° 2θ. The XRD patterns of solids prepared with 10 and 20 wt% surfactant solutions are similar, and different from those prepared with surfactant concentrations of 30 and 40 wt%, with the X-ray diffraction peaks observed at higher angle increasing in relative intensity at the higher surfactant concentrations. SEM and TEM reveal that changes in the morphology of the phases are occurring as the surfactant concentration is increased (Fig. 5 and 6). The morphology of the mesoporous materials changes from solid spheres with diameters ranging from 1 to 20 μm (using 10 wt% surfactant concentration), through a mixture of rhombic dodecahedral particles of 1–10 μm in size and larger particles with no distinct shape or hexagonal prisms (20, 30 wt% surfactant concentration), to hexagonal prisms 2–8 μm across (40 wt% surfactant concentration). The observed solid sphere morphology of the particles formed using the 10 wt% aqueous surfactant solutions has been reported previously[32] for silica–surfactant mesophases under acidic conditions where the surface tension of the growing liquid crystal droplet is proposed to be the controlling feature. The presence of the hexagonal prismatic morphology in the samples prepared using 40 wt% surfactant solution is clear evidence for the formation of a hexagonal phase, and SEM indicates that this phase is pure at this surfactant concentration. In contrast, although rhombic dodecahedral morphology is associated with cubic symmetry, the formation of other morphologies when using 20 and 30 wt%

surfactant indicates a mixture of two phases at lower surfactant concentrations, including cubic and hexagonal phases. The latter is more abundant as the concentration is increased, suggesting a shift towards a pure hexagonal $P6_3/mmc$ phase.

Fig. 6(a) shows an HRTEM image of the solid spheres obtained using 10 wt% C16-3-1 surfactant, similar to those reported for SBA-2 synthesised in basic media, showing stacking faults typical of the SBA-2 family. This phase is, therefore, identified as SBA-2(acid). It is possible to index the XRD pattern [Fig. 4(b)] of these spheres on a hexagonal unit cell ($P6_3/mmc$) with the unit cell parameters given in Table 2.

The HRTEM image of the sample synthesised with 40 wt% surfactant [Fig. 6(d)] shows some well-ordered regions in the hexagonal close-packed stacking sequence, as well as some stacking faults. No cubic stacking sequences were observed in our HRTEM studies, suggesting that this is a hexagonal end-member phase related to SBA-2. This phase is denoted STA-10 (St. Andrews-10). It is possible to index the XRD pattern [Fig. 4(e)] of this phase on a hexagonal unit cell ($P6_3/mmc$) with the unit cell parameters listed in Table 2.

HRTEM microscopy on the materials synthesised with 20 and 30 wt% C16-3-1 solutions [Fig. 6(b) and (c), respectively] indicates that the well-defined rhombic dodecahedral particles give images typical of the [210] patterns reported for SBA-1. The insets show the simulated electron diffraction pattern (beam direction [210]) of the image in question. These and other electron diffraction patterns have been indexed on the basis of a primitive cubic unit cell. These images are consistent with a cubic unit cell related to SBA-1,[10,11,17] although the observed X-ray diffraction pattern is not identical to that of SBA-1. More convincing evidence for the synthesis of SBA-1 using the C16-3-1 surfactant is provided by experiments using a 20 wt% aqueous solution of surfactant with decreasing concentrations of silicate (Table 3). The XRD patterns of the resulting mesoporous calcined solids change to resemble that typical of SBA-1 (Fig. 7) with an increase in the *d*-spacing of the most intense diffraction peak. The SBA-1 phase prepared under these conditions shows well-defined rhombic dodecahedral morphology, with particle dimensions of 1–20 μm (Fig. 8). This morphology is consistent with the point group $m\bar{3}n$ and has been reported previously for SBA-1 and its large pore equivalent, SBA-6, by Sakamoto *et al.*[13] HRTEM images of this sample looking down [210] reveal extensive regions of ordered material. A typical HRTEM image of SBA-1, prepared using the usual CTEABr surfactant, is also shown in Fig. 8 for comparison.

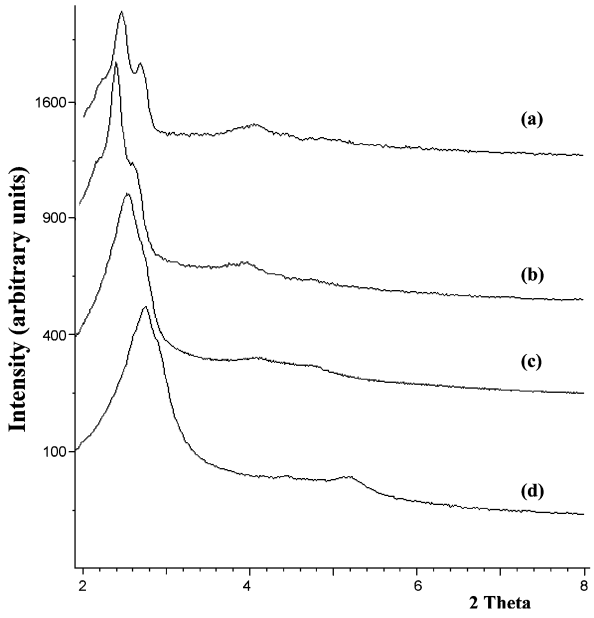

Fig. 7 Powder XRD patterns of calcined samples synthesised using 20 wt% surfactant with varying amounts of TEOS. Surfactant/TEOS weight ratios: (a) 0.4; (b) 0.6; (c) 0.8; (d) 1.

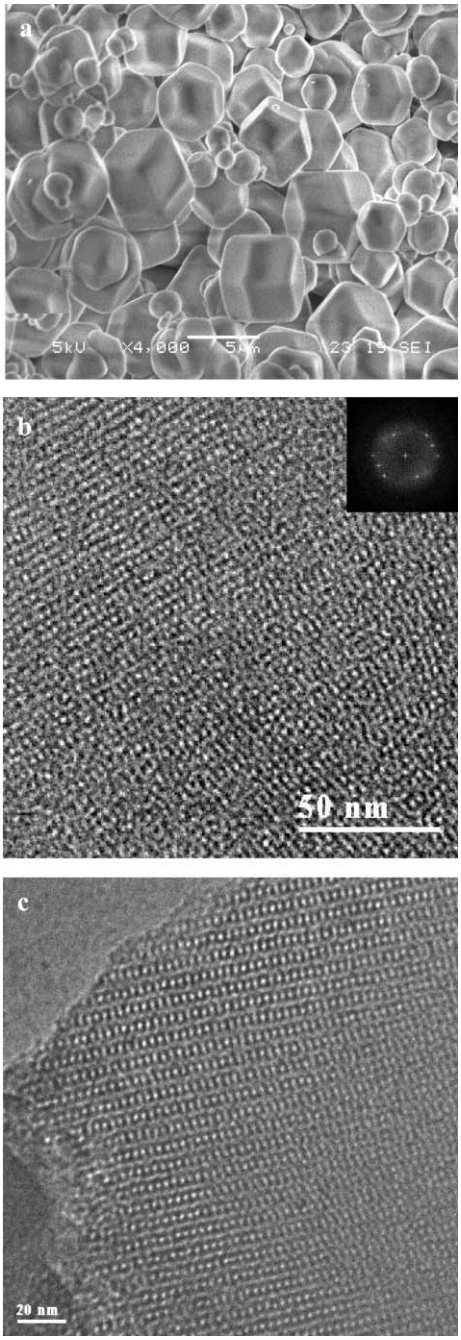

Fig. 8 (a) Typical SEM image of the rhombic dodecahedral particle morphology of SBA-1, synthesised under acidic conditions with C16-3-1 surfactant. (b) TEM image of a large ordered region looking down the [210] direction of this material; the inset shows the FT diffraction pattern of a selected area of the image. (c) TEM image of SBA-1 synthesised with CTEABr surfactant.

The solid-state DP MAS ^{29}Si NMR spectra (Fig. 9) give better resolved Q^4 [$Si(OSi)_4$], Q^3 [$Si(OSi)_3OH$] and Q^2 [$Si(OSi)_3$-OH] resonances for samples of SBA-1 prepared using both C16-3-1 and CTEABr surfactants than for samples of SBA-2 (and STA-10) prepared using C16-3-1. This indicates that there is a narrower range of environments present in SBA-1 than in the SBA-2 family of solids.

The adsorption branches of nitrogen, cyclopentane and mesitylene isotherms for SBA-2RT, SBA-2(acid), SBA-1(C16-3-1) and STA-10 are shown in Fig. 3. The nitrogen and cyclopentane adsorption and desorption branches display no

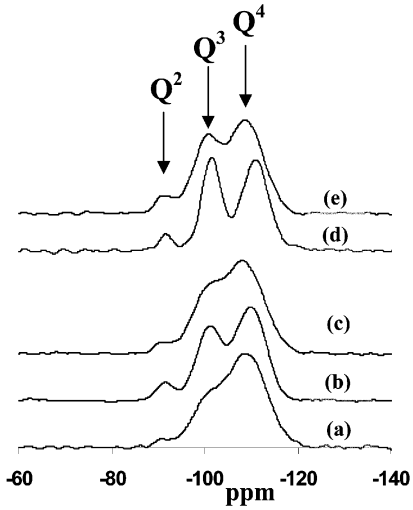

Fig. 9 DP MAS ^{29}Si NMR spectra of calcined mesoporous materials synthesised using a variety of conditions: (a) SBA-2RT, basic conditions, 1 wt% C16-3-1, r.t.; (b) SBA-2(acid), acidic conditions, 10 wt% C16-3-1, −4 °C; (c) STA-10, acidic conditions, 40 wt% C16-3-1, −4 °C; (d) SBA-1(CTEABr), acidic conditions, CTEABr surfactant, −4 °C; (e) SBA-1(C16-3-1), acidic conditions, 20 wt% C16-3-1, −4 °C. The resonances from silicon atoms surrounded by two, three and four (–O–Si) linkages are labelled Q^2, Q^3 and Q^4, respectively.

hysteresis, but the mesitylene data do (for full data, including adsorption and desorption isotherms, see ESI). The total pore volume, as measured by nitrogen uptake, is similar (45–50 wt%) for all these solids, and is higher than that observed for the SBA-2 prepared under basic conditions. Values for the specific surface area, pore size distribution and pore volume are summarised in Table 4. Whereas SBA-2RT has a pore window between 3 and 4 Å (nitrogen is admitted to the internal pore space, whereas *n*-hexane is not), the materials prepared under acidic conditions have pore connectivity through larger windows. The well-defined hexagonal prisms of the end-member phase STA-10 are able to adsorb cyclopentane (5 Å) but not mesitylene (8 Å). The solid spherical particles of SBA-2(acid) adsorb cyclopentane and mesitylene, although uptake of these hydrocarbons is at a lower level than observed for SBA-1 prepared with the same template.

This series of experiments shows that the three-dimensional hexagonal ($P6_3/mmc$) phase and the cubic ($Pm\bar{3}n$) phase can be prepared as silica–surfactant composites under highly acidic conditions using the dicationic surfactant C16-3-1. This is the first observation of the formation of SBA-1 using this surfactant. Whether the cubic or hexagonal phase is the dominant product depends on the composition of the synthesis mixture. The large head group volume of the C16-3-1 surfactant is known to favour micelles with high surface curvature, and both SBA-1 and SBA-2 form with three-dimensional ordering of micelles of this type.

The adsorption studies of nitrogen, cyclopentane and mesitylene reveal, for the first time, details of the sizes of the windows connecting the large cages in both SBA-1 and SBA-2. SBA-1 samples prepared with both the C16-3-1 and CTEABr surfactants are able to adsorb large volumes of mesitylene, indicating pore windows with diameters in excess of *ca.* 8 Å. The window size of the three-dimensional hexagonal mesoporous silicas prepared using C16-3-1 as a template varies strongly with the synthesis conditions. SBA-2 prepared under basic conditions possesses very small windows (<4 Å), whereas those materials synthesised under acidic conditions are able to adsorb cyclopentane and, in the case of SBA-2(acid), mesitylene. The window sizes of the members of the SBA-2 family of three-dimensional solids prepared at different pHs are not always directly proportional to their unit cell sizes: samples of SBA-2 prepared under basic conditions have larger unit cell values, but smaller window sizes, than the materials prepared under acidic conditions [SBA-2(acid), STA-10 and SBA-1(C16-3-1)]. This difference may be due to the fact that silicate condenses as a thin layer between globular micelles under basic conditions, but is removed from the region between micelles when they agglomerate under the acidic conditions that give SBA-1 and the 3-D hexagonal phase. Representations of the postulated interactions between the surfactant and silicate wall under acidic and basic conditions are shown in Fig. 10.

Conclusions

In the presence of high concentrations of the dicationic surfactant C16-3-1, under acidic conditions and at low temperatures, the mesoporous silica SBA-1 and the SBA-2 family of silicas (based on close packing of spheres) have been synthesised. HRTEM, SEM and XRD studies confirm unambiguously the formation of SBA-1 with the C16-3-1 surfactant for the first time, and have revealed the formation of STA-10, a hexagonal mesostructure which is the hexagonal ($P6_3/mmc$) polymorph of SBA-2 without significant cubic close-packed sequences. Vapour adsorption studies show that SBA-1 prepared with C16-3-1 surfactant has a high pore volume which is accessible to mesitylene, indicating a window size of more than *ca.* 8 Å. Adsorption studies also show that the window size of the three-dimensional hexagonal phase is strongly dependent on the conditions of its synthesis, with basic conditions yielding materials with pores of less than *ca.* 4 Å, while materials prepared in acidic media are able to adsorb cyclopentane and, in some cases, mesitylene.

Acknowledgements

This work has been supported by an EPSRC grant (A. E. G. B.). The authors would like to thank Dr Christine Göltner (Bristol University), Dr Wuzong Zhou (St. Andrews University), and

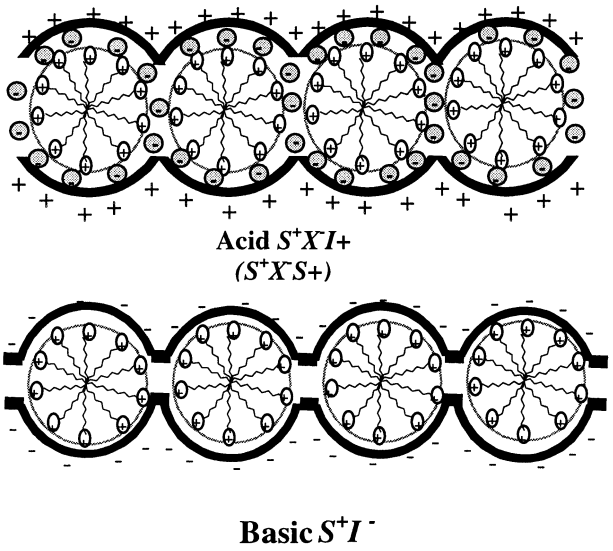

Fig. 10 Proposed interactions between the inorganic silicate framework and the surfactant micelle under acidic and basic conditions. Charges outside the cages represent the charged inorganic species (+ve and −ve for syntheses conducted in acidic media and basic media, respectively). Under acidic conditions, the micellar surface consists of positively charged surfactant headgroups balanced by halide counterions (represented by the negatively charged small grey spheres). Under basic conditions, the positively charge micellar surface is balanced directly by the inorganic species.

Miss Chrystelle Egger and Professor Michael Anderson (UMIST, Manchester) for helpful discussions.

References

1 C. T. Kresge, M. E. Leonowicz, W. J. Roth, J. C. Vatuli and J. S. Beck, *Nature*, 1992, **359**, 710.
2 J. S. Beck, J. C. Vartulli, W. J. Roth, M. E. Leonowicz, C. T. Kresge, K. D. Schmitt, C. T-W. Chu, D. H. Olson, E. W. Sheppard, S. B. McCullen, J. B. Higgins and J. L. Schlenker, *J. Am. Chem. Soc.*, 1992, **114**, 10834.
3 A. Corma, *Chem. Rev.*, 1997, **97**, 2373.
4 J. M. Thomas, *Angew. Chem., Int. Ed.*, 1999, **38**, 3589.
5 U. Ciesla and F. Schüth, *Microporous Mesoporous Mater.*, 1999, **27**, 131.
6 D. Zhao, Q. Huo, J. Feng, B. F. Chmelka and G. D. Stucky, *J. Am. Chem. Soc.*, 1998, **120**, 6024.
7 A. Monnier, F. Schüth, Q. Huo, D. Margolese, R. S. Maxwell, G. D. Stucky, M. Krishnamurty, P. Petroff, A. Firouzi, M. Janicke and B. F. Chmelka, *Science*, 1993, **261**, 1299.
8 M. W. Anderson, *Zeolites*, 1997, **19**, 220.
9 C. Landry, S. Tolbert, K. Wallis, A. Monnier, G. Stucky, P. Norby and J. Hanson, *Chem. Mater.*, 2001, **13**, 1600.
10 Q. Huo, R. Leon, P. M. Petroff and G. D. Stucky, *Science*, 1995, **268**, 1334.
11 Q. Huo, D. I. Margolese and G. D. Stucky, *Chem. Mater.*, 1996, **8**, 1147.
12 M. J. Kim and R. Ryoo, *Chem. Mater.*, 1999, **11**, 487.
13 S. Che, Y. Sakamoto, O. Terasaki and T. Tatsumi, *Chem. Mater.*, 2001, **13**, 2237.
14 W. Zhou, H. M. A. Hunter, P. A. Wright, Q. Ge and J. M. Thomas, *J. Phys. Chem. B*, 1998, **102**, 6934.
15 H. M. A. Hunter, A. E. Garcia-Bennett, I. J. Shannon, W. Zhou and P. A. Wright, *J. Mater. Chem.*, 2002, **12**(1), 20.
16 M. Kruk, M. Jaroniec, R. Ryoo and J. M. Kim, *Chem. Mater.*, 1999, **11**, 2568.
17 Y. Sakamoto, M. Kaneda, O. Terasaki, D. Y. Zhao, J. M. Kim, G. D. Stucky, H. J. Shin and R. Ryoo, *Nature*, 2000, **408**, 449.
18 Y. Sakamoto, I. Diaz, O. Terasaki, D. Y. Zhao, J. Perez-Pariente, J. M. Kim and G. D. Stucky, *J. Phys. Chem. B.*, 2002, **106**, 3118.
19 S. Che, Y. Sakamoto, O. Terasaki and T. Tatsumi, *Chem. Mater.*, 2001, **13**, 2237.
20 H. M. A. Hunter and P. A. Wright, *Microporous Mesoporous Mater.*, 2001, **43**, 361.
21 M. Clerc, *J. Phys. II*, 1996, **6**, 961.
22 J. M. Kim, Y. Sakamoto, Y. K. Hwang, Y-U. Kwon, O. Terasaki, S. E. Park and G. D. Stucky, *J. Phys. Chem. B*, 2002, **106**, 2552.
23 E. P. Barrett, L. G. Joyner and P. H. Halenda, *J. Am. Chem. Soc.*, 1951, **73**, 373.
24 S. H. Tolbert, T. E. Schäffer, J. Feng, P. K. Hansma and G. D. Stucky, *Chem. Mater.*, 1997, **9**, 1962.
25 D. Zhao, P. Yang, D. I. Margolese, B. F. Chmelka and G. D. Stucky, *Chem. Commun.*, 1998, 2499.
26 S. Besson, T. Gacoin, C. Jacquiod, C. Ricolleau, D. Babonneau and J.-P. Boilot, *J. Mater. Chem.*, 2000, **10**, 1331.
27 P. Ravikovitch, G. Haller and A. Neimark, *Adv. Colloid Interface Sci.*, 1998, **76–77**, 203.
28 P. Ravikovitch and A. Neimark, *Langmuir*, 2002, **18**, 1550.
29 R. Zana, M. Benrraou and R. Rueft, *Langmuir*, 1991, **7**, 1072.
30 C. G. Göltner, B. Smarsly, B. Berton and M. Antonietti, *Chem. Mater.*, 2001, **13**, 1617.
31 Digital Micrograph 3.4, Gatan, Inc., Pleasanton, CA, USA, November 1999.
32 H. Yang, G. Vovk, N. Coombs, I. Sokolov and G. A. Ozin, *J. Mater. Chem.*, 1998, **8**, 743.
33 S. J. Gregg and K. S. W. Sing, *Adsorption, Surface Area, and Porosity*, Academic Press, London, 1982.